CogniDaVinci: Towards Estimating Mental Workload Modulated by Visual Delays During Telerobotic Surgery – An EEG-based Analysis

Satyam Kumar[1,*], Deland H. Liu[1,*], Frigyes S. Racz[2,*], Manuel Retana[3,*], Susheela Sharma[3], Fumiaki Iwane[1,2], Braden P. Murphy[3], Rory O'Keeffe [4], S. Farokh Atashzar[4,†], Farshid Alambeigi[3,†], and José del R. Millán[1,2,†]

***Abstract*— Communication latency in any delicate telerobotic operation (such as remote surgery over distance) would impose a significant challenge due to the temporal degradation of visual perception and can substantially affect the outcomes. Less is known, however, about the neurophysiological basis of how operators adapt/react to delayed visual feedback. Identification of such neural markers might provide novel ways for future applications to monitor the mental workload (MW). In this study, we recorded electroencephalography (EEG) data from nine users while performing a peg transfer task using the da Vinci Research Kit with three levels of induced visual delay in the video feedback. Our results suggest that spectral EEG-based features can provide markers of the operator's MW modulated by arbitrary visual delay. We also show that the exposure to different visual delays could be successfully classified/detected solely from EEG data, using a Riemannian geometry-based classifier, which highlights the utility of EEG signals for detecting the effect of visual delay on brain activity.**

I. INTRODUCTION

Development of robotic teleoperation techniques has paved the way for remote surgery [1]–[3]. Robot-assisted surgery (RAS) allows surgeons to perform remote operations when the subjects are located miles away [4], and even ultimately in outer space [5]. However, in such scenarios one may face limitations imposed by communication latency — or "time delay" — in the visual feedback, which can drastically affect the performance of a surgeon. This delay in visual feedback introduces additional demand on cognitive processing, resulting in increased mental workload (MW) [1], [6], [7].

MW and other cognitive states of the operator in an RAS setting have been typically assessed via various *indirect* markers including questionnaires such as the NASA Task Load Index and the Surgery Task Load Index (e.g., [8]–[10]), expert observations (e.g., [11]), heart rate variability [8], or eye-tracking markers (e.g., [12]). For example, using such *indirect* markers, it has been studied how delayed video feed in a laparoscopic procedure and RAS could increase the MW of the surgeon [8], [13], [14]. In addition, Anvari et al. [15] explored the effect of induced delay on the task completion time and error rates at latencies of 150 ms and 500 ms. In another study, Madder et al. [16] investigated the impact of video and audio feedback latency on the telestenting performance during a coronary artery wiring task.

While various robotic approaches have been developed in the past (e.g., [1], [3], [6], [17]) to mitigate the MW issue, as assessed through the above-mentioned *indirect* analyses, it is much less explored how direct neurophysiological markers can be used to objectively quantify, monitor, and evaluate the level of MW. Therefore, the main focus of this present study was to investigate the possibility of capturing and decoding the neural signatures of increased MW and related cognitive states induced by the delayed visual feedback.

Unlike the aforementioned indirect MW assessment metrics, electroencephalography (EEG) provides a flexible, effective, and real-time way of recording ongoing neural processes. Moreover, a recent study suggests that EEG provides better markers for MW assessment than other physiological variables (e.g., heart rate variability or electrodermal activity [18]). Various approaches have been proposed in order to extract direct neural correlates of MW from EEG in generic applications, with most EEG-based studies utilizing band-limited power spectral density (PSD) to characterize ongoing cortical activity. In the context of RAS, some initial efforts have also been reported in the literature (e.g., [19], [20]).

Overall, it should be highlighted that to the best of our knowledge, the effect of visual delay in a telemanipulation setting has not been assessed using EEG in the past. Therefore, identifying biomarkers of MW caused by various delay conditions might pave the way for more efficient telesurgery, tackling the increased MW of surgeons in the presence of feedback-delay. Therefore, this paper identifies neural correlates of delayed visual feedback in an RAS scenario. The robotic hardware is based on a da Vinci Research Kit (dVRK) [21]. We recorded EEG data from 9 subjects while performing a pick-and-place task using the dVRK under three different delay conditions. We carried out PSD analysis to assess plausible neural markers associated with the various delay exposure. We also show that the exposure to different visual delays could be detected solely from EEG data, using a Riemannian geometry-based classifier. The classification

*These authors contributed equally.

†Equal senior authorship.

[1]Department of Electrical and Computer Engineering, The University of Texas at Austin, Austin, TX, USA. E-mail: {satyam.kumar, deland.liu}@utexas.edu, jose.millan@austin.utexas.edu

[2]Department of Neurology, The University of Texas at Austin, Austin, TX, USA. Email: fsr324@austin.utexas.edu

[3]Walker Department of Mechanical Engineering, Texas Robotics, The University of Texas at Austin, Austin, TX, USA. E-mail: {manuel.retana, sheela.sharma, bradenpmurphy}@utexas.edu, Farshid.Alambeigi@austin.utexas.edu

[4]Department of Electrical and Computer Engineering, and Department of Mechanical and Aerospace Engineering, New York University, NY, USA. E-mail: rory.okeeffe@nyu.edu , f.atashzar@nyu.edu

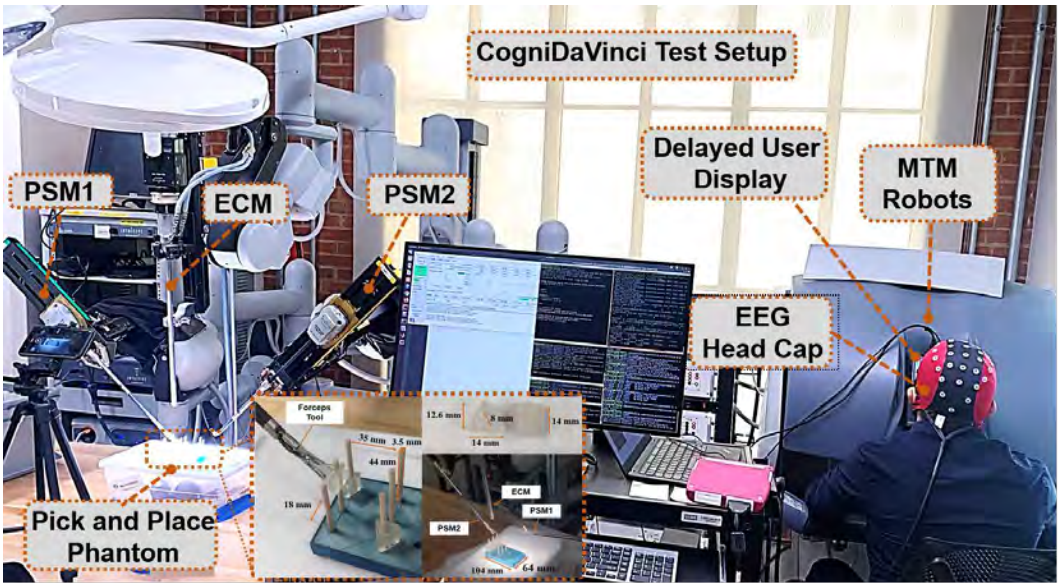

Fig. 1. The experimental setup includes the human test subject wearing an EEG Head Cap while manipulating the MTMs in surgeon console controlling the PSMs and looking at a display showing the visual feedback coming from the endoscopic Camera, with and without the presence of a synthetic delay. Figure also shows the custom-designed pick and place phantom.

study, highlights the information content of EEG signals for detecting the effect of visual delay on brain activity.

II. Experiments and Methodology

A. Participants and Experimental Protocol

Our study was conducted in accordance with the relevant guidelines of the Declaration of Helsinki. Participants signed an informed consent before the experiment. The study was approved by UT Austin's ethics committee (ID: 2020030073-MODCR01). We enrolled nine volunteers (1 female and 8 males) with mean age 25 ± 0.7 years, all right-handed. All participants had previous experience in the Peg Transfer Task and handling the dVRK. Subjects controlled the patient side manipulator (PSM) using their right hand. Subjects completed 12 distinct three minute long runs of the Peg Transfer Task (see below) with approximately 2 minutes of rest between task periods. In each run, subjects performed the task with visual feedback being delivered either in real time with no delay (`ND`), short delay of 150 ms (`SD`) or long delay of 500 ms (`LD`). Participants completed 4 runs of each condition in a randomized order.

B. Experimental setup and Peg Transfer Task

For our studies, we chose the peg transfer surgical task– a classic fundamentals of laparoscopic surgery task [22]– and used the dVRK [21] to conduct our experiments. The dVRK has been used extensively in the medical robotics research community and has open source electronics and software (cisst/SAW libraries) developed by the researchers at the Johns Hopkins University. The system has one stereo camera installed on one Endoscopic Camera Manipulator (ECM) to control the movement of camera and endoscopic view. Two master tool manipulators (MTMs) allow a surgeon to simultaneously teleoperate two patient side manipulators (PSMs). Interchangeable tools are installed on the PSMs. The PSM used in these experiments utilizes an EndoWrist® Pro-Grasp™ Forceps (Intuitive surgical, Inc., California, USA) tool, which has two 16 mm fingers for holding the fabricated phantoms. Typically, the da Vinci robotic system operates three distinct PSMs, but for our experiments, we limited our scope to two PSMs. Also, instead of using the stereo visual feedback provided by the endoscope in the MTM console, we interfaced a 5 inch HDMI display with 800×480 mini LCD screen (ELECROW Inc.) with the MTM and displayed the video feed provided by the endoscope on this monitor. We also leveraged Robot Operating System (ROS) and dVRK software to utilize the endoscope video feed and create a separate node to inject a custom delay and simulate various visual delay conditions for the operator. For our peg transfer experiments, we also developed a custom peg transfer phantom (shown in Fig. 1) including triangular deformable tissue-like phantoms made out of Elastic 50A resin using the Form 3 (Formlabs Inc.) Stereolithography 3D printer. The experimental setup is also shown in Fig. 1.

The task consisted of transferring a set of triangular phantoms from a vertical base peg to the goal peg as fast as possible (see the inset in Fig. 1) via dVRK using a single MTM with and without the presence of a synthetic visual delay. Each run was scored as follows: the operator received 1 points for successful transfers and 0.5 points for unsuccessful attempts (e.g., dropped phantom). During the task, if the peg fell, it was expected from the users to pick the phantom up and transfer it to the goal peg or switch to another phantom at their base peg. Note that task performance data was only available for 8 out of 9 subjects (all but subject 1).

C. EEG recording and pre-processing

Scalp EEG was recorded at 512 Hz using an eego system (ANT Neuro, Netherlands) from 32 cortical regions in standardized 10-10 International System locations (refer to Fig. 5C for list of electrodes). All subsequent data processing and analyses were carried out in Matlab (MathWorks, Natick, MA) using custom scripts and functions of the EEGLAB toolbox [23]. EEG was filtered in the frequency band [4-30] Hz with a 5^{th} order non-causal Butterworth filter to avoid movement-related slow cortical potentials and high frequency noise. Filtered EEG was then re-referenced to the common average electrode. The EEG signals for each visual feedback condition (`no delay (ND)`, `short delay (SD)`, `long delay (LD)`) were epoched into trials using a sliding window of 3 s at 1 s step size. Trials were then concatenated per condition. Only trials from the first minute of each recording were included to avoid plausible effects of habituation and fatigue. Furthermore, trials with filtered EEG signal amplitude above/below ± 100 μV were considered artifactual and excluded from further analyses.

D. EEG spectral power analysis

We conducted spectral power analysis to study EEG spectral modulations while subjects performed the peg transfer task. For each subject, power spectral density (PSD) at each electrode and epoch was estimated using Welch's algorithm at 1 s windows with 500 ms overlap. From the PSD estimates, the total band limited power (BLP) was estimated in each epoch via integration, and finally averaged over all the trials in each visual feedback condition. BLP was computed in the following standard frequency ranges: θ: 4–8 Hz; α: 8–13 Hz; and β: 13–30 Hz. For each subject, the differences in averaged BLP values between the visual feedback delay conditions were also computed at all electrodes.

E. Classification Approach

Riemannian geometry-based classifiers have recently shown promising results for EEG-based brain-machine interfaces [24]. In the Riemannian geometry framework, covariance matrices of band pass filtered signals are directly used as features for building the classifiers. These covariance feature matrices encode both the spatial (lower/upper triangulars) and power (main diagonal) information of the bandpass filtered signal. Minimum distance to Riemannian Mean (MDRM) is one of the most commonly used, robust Riemannian geometry classifier approaches [25]. MDRM works on the principle of nearest neighbor classification and classifies the covariance features directly on the Riemannian manifold. We used 3 s windows with a step size of 1 s on the first 1 minute of broadband ([4-30] Hz) EEG data from the different delay conditions to estimate covariance matrices [26]. The estimated covariance matrices of different delay conditions were then used to build the MDRM classifier. The chance level for binary class classification was estimated individually for each testing fold by using the inverse binomial distribution using a $p = 0.05$ and the total number of trials in each of the testing folds (see [27] for details).

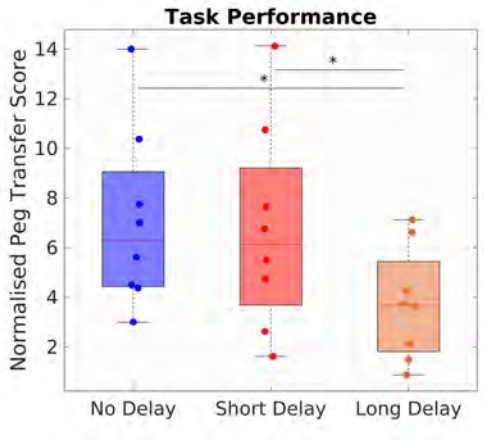

Fig. 2. Box plot of the distribution of peg transfer scores in different delayed feedback conditions. Box edges mark 75$^{\text{th}}$ and 25$^{\text{th}}$ percentiles, while horizontal lines correspond to the median. * : $p < 0.05$.

F. Neurophysiological Feature Discriminancy

We explored, which BLP features carry the most discriminating power between the various delay conditions. For this purpose we chose the Fisher score-based feature discriminancy criterion to select subject-specific discriminant features [28]. The Fisher score $S(y_i)$ for a given feature y_i $(i = 1 \cdots m * N_c)$, where m is number of frequency bins and N_c is number of channels, is computed by the equation:

$$S(y_i) = \frac{\sum_{k=1}^{K} \left| \mu_{y_{i,k}} - \mu_{y_i} \right|}{\sqrt{\sum_{k=1}^{K} \sigma^2_{y_{i,k}}}} \tag{1}$$

where $\mu_{y_{i,k}}$ and $\sigma^2_{y_{i,k}}$ are the mean and variance, respectively, for a given feature over all samples for a given class $k \in \{1, 2 \cdots K\}$, and μ_{y_i} is the mean across all the samples of feature y_i. We ranked the features using (1) and visualised the 20 most discriminant features.

III. RESULTS

A. Task performance

Fig. 2 reports the task performance metric Peg Transfer Score normalised by the number of runs for each visual delay condition. One-way repeated measures analysis of variance (ANOVA) indicated a significant main effect of visual feedback delay on performance ($p = 0.00068$, Greenhouse-Geisser-corrected, Mauchly's $p = 0.4993$). Post-hoc pairwise comparisons (all p-values Bonferroni-adjusted for multiple comparisons) indicated that peg transfer performance decreased significantly in the `LD` condition (3.7344 ± 2.2643) when compared to the `ND` (7.0781 ± 3.6240, paired t-test, $p = 0.0019$) and `SD` (6.7240 ± 4.1416, paired t-test, $p = 0.0197$) conditions. No difference was found between `ND` and `SD`.

B. Spectral power analysis

Previous studies have proposed increase in frontal θ [29]–[31], parietal θ [32] and decrease in occipital α power [32] as plausible neural markers of MW. With this in mind, we were focusing on these regions throughout BLP analyses (Fig. 3). As frontal theta BLP data (averaged over electrodes AF3,

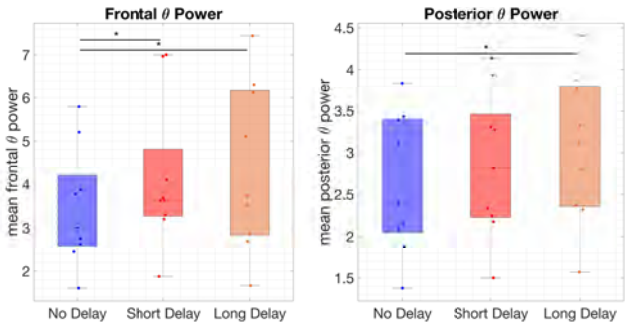

Fig. 3. Box plot of the average θ spectral power (4–8 Hz) in the three different delayed feedback conditions at frontal region (left) and posterior region (right). *: $p < 0.05$.

AF4, F1, F3, Fz, F2 and F4) did not satisfy the normality criterion (Lilliefors test, $p > 0.05$) we used Friedman and the Wilcoxon signed rank tests. The p-values from all post-hoc comparisons were adjusted using Bonferroni's method. Friedman's test identified a significant main effect ($p = 0.0164$) of visual input delay on frontal θ power (Fig. 3, left panel). Post-hoc paired Wilcoxon signed rank tests revealed a significant increase in mean θ power at frontal regions when subjects performed the task with SD (4.1540 ± 1.7184, $p = 0.0234$) and LD (4.3866 ± 1.9457, $p = 0.0234$) with respect to ND (3.4552 ± 1.3519).

Furthermore, repeated measures ANOVA identified a significant main effect ($p = 0.02526$, Greenhouse-Geisser corrected, Mauchly's $p = 0.1398$) of delay condition on posterior θ power (averaged over regions PO3, POz and PO4), too (Fig. 3, right panel). Paired t-tests revealed a significant increase in mean θ BLP at posterior regions in LD (3.0620 ± 0.8926, $p = 0.0410$) with respect to ND (2.6306 ± 0.8359), while the increase in SD was found only marginally significant (2.8581 ± 0.8749, $p = 0.0506$) (Fig. 3). No differences in frontal and parietal θ power were found between SD and LD. Note that parietal θ BLP data satisfied the normality criterion (Lilliefors test, $p < 0.05$) and all post-hoc p-values are Bonferroni-adjusted.

Delayed feedback with (SD or LD) led to a decrease in mean α power relative to ND at occipital sites (O1, O2) (4.7267 ± 2.0154, 5.0988 ± 2.4180 and 5.5738 ± 3.2795 for LD, SD and ND, respectively), however this decrease was not statistically significant.

Fig. 4 shows the grand average topographic maps of the differences in θ, α and β BLP between LD and ND, and SD and ND conditions. The spatial distributions of the observed differences further confirm our findings described above. We also observed an increase in β BLP over the left frontal and central regions in LD and left central and posterior regions in SD, however post-hoc analysis did not identify any significant differences in β BLP between the various delay conditions.

C. EEG classification analysis

We performed subject-wise cross-validation (CV) between pairs of the different delay conditions ND−SD, ND−LD and SD−LD. Note that during pairwise CV, only covariance

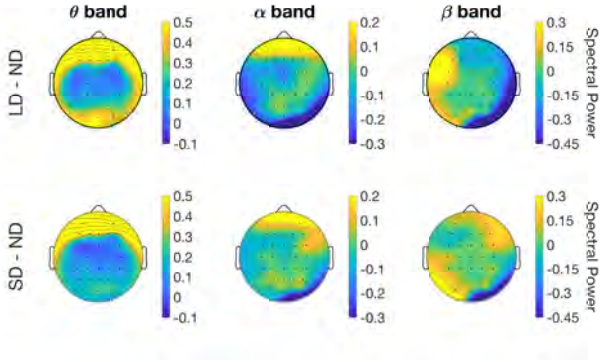

Fig. 4. Topological analysis of the average spectral power differences between LD and ND conditions (LD − ND), and SD and ND conditions (SD − ND), in θ (4–8 Hz), α (8–13 Hz) and β (13–30 Hz) rhythms modulations. LD: long delay; ND: no delay; SD: short delay.

features from the training folds were used to build the classifier for each partition. The reported cross-validation accuracies correspond to the average across all the folds for each pairwise comparison (Fig. 5A). For ND vs LD, 4 subjects out of 9 had a better than chance level performance, with average across the subjects of (68.58 ± 5.96 %). For SD vs LD, 4 subjects achieved a better than chance level performance, with average across the subjects of (63.41 ± 4.16 %). Taken together, 6 out of 9 subjects reached a statistically significant performance above chance level for at least one pairwise comparison.

D. Discriminant Features

Fig. 5B illustrates the cumulative distribution of top 20 most discriminant features across all the 9 subjects between ND vs LD conditions as a function of frequency bins and channels. We observed that theta-band (4-8 Hz) features were found discriminative the most frequently and contributed to 58.33% of the top 20 features.

IV. DISCUSSION

The performance of subjects in the peg transfer task show that LD has significantly lowered ($p < 0.05$) Peg transfer score compared to SD and ND. This finding is consistent with previous task-oriented behavioral findings where it was observed that increasing visual feedback delay decreases task performance [13].

Frontal θ spectral power has been proposed previously as a distinct neural signature of MW. For example, frontal θ power was shown to increase with task difficulty [29], cognitive demand in multi-tasking environments [30] and working memory load [31]. θ power increase at parietal sites, as observed in LD condition (Fig. 3), has also been associated with increased workload demands [32]. Moreover, previous studies have linked increased MW to increased α desynchronization amplitude over parietal and occipital areas [32]. Decrease in occipital α power may also reflect an increase in visual information processing and allocation of attentional resources during the delayed feedback [33]. These findings are in line with our observations from Fig. 3 and 4.

In addition, established evidence from literature has suggested θ band modulations in the anterior cingulate cortex

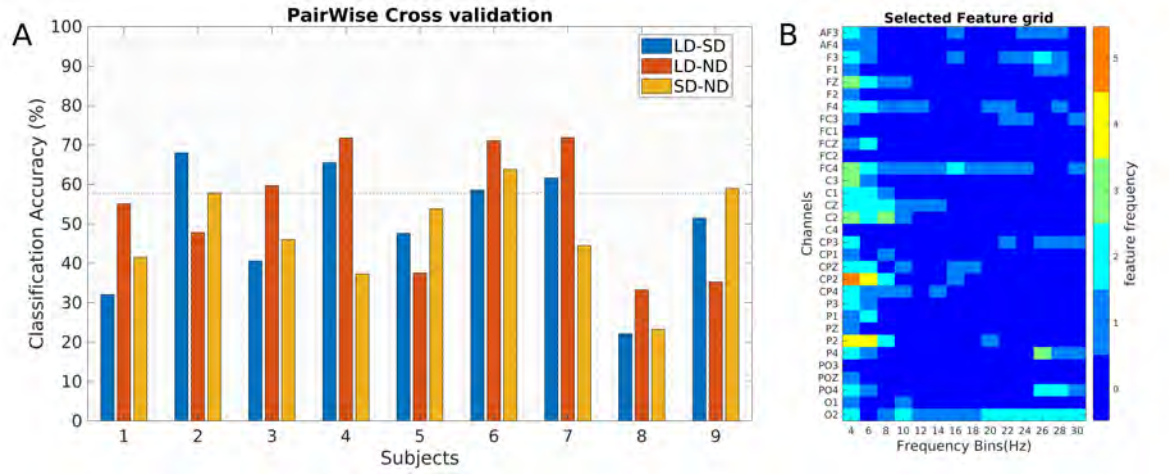

Fig. 5. A) Pairwise cross-validation performance, dashed black line correspond to chance level classification performance. B) Frequency of top-20 features selected using Fisher score discriminancy criteria, over all subjects. LD: long delay; ND: no delay; SD: short delay.

(ACC) as the neural correlate involved in monitoring of erroneous events, feedback and expectation mismatch [34]. Therefore, expectation mismatch as a result of the visual feedback delay might induce θ power increase at frontal and fronto-central locations. Indeed, delayed feedback conditions led to an increase in θ power at Fz (3.5483 ± 1.3100, 3.3918 ± 1.0775 and 2.9681 ± 0.9511 for LD, SD and ND, respectively) and FCz (2.0897 ± 0.7364, 1.9972 ± 0.7290 and 1.9630 ± 0.7462 for LD, SD and ND, respectively) locations. Even though these differences were found not statistically significant, they may still approach significance with a larger subject group.

Neural markers discussed above, in particular those associated with MW, can be observed in Fig. 4 even in SD. This finding is reinforced in Fig. 5B, where pairwise CV classification results SD vs ND were above chance in 2 out of 9 subjects. Though we did not record subjective evaluations, according to previous evidence on a similar task, subjects cannot perceive the added visual delay at this latency (SD: 150 ms) [16]. This suggests that visual feedback delays might have increased MW even when the operators did not consciously perceive them.

In our exploratory pairwise CV analysis we found that for some of the subjects LD vs ND classification could be performed with fairly high confidence ($accuracy > 70\%$ in three cases, Fig.5A). Classification performances could most likely be further improved by collecting more runs (hence more data) for the various delay conditions, thus building more robust decoding models. Moreover, the users operating the da Vinci robot could be trained in a closed-loop feedback setting to generate better discernable patterns for the three delay conditions. Fig. 5B presents the most discriminative features (across all subjects) ranked according to their Fisher score-based discriminatory criteria. Most discriminant features were found in low θ components, suggesting θ rhythm modulations as neural markers of cognitive processes involved in the task. Furthermore, we observed some discriminant features in the β band at posterior and occipital areas, plausibly responsible for visual information processing.

Importantly, Fig. 4 shows that spectral power differences in the α and β bands over the motor cortex (FC, C and CP line electrodes) were in most cases practically zero in comparison to θ power changes at the frontal regions. There was an increase in β power in LD feedback at the contralateral sensorimotor regions (FC3, C3), which might possibly be a result of slower and fewer hand movements as a result of delayed feedback. Since movement generation is generally characterised by α and β sensorimotor rhythms [35], the lack of changes in α and β power at other sensorimotor locations supports the notion that neural correlates observed here were not primarily elicited by the motor movements from interaction with the robot, but instead by ongoing cognitive processes.

In terms of study limitations, it must be mentioned that our pilot study cohort only included 9 subjects. Therefore, one of our main future goals is to increase the sample size so that we can validate the results presented here on a more representative population. Also, classification was carried out offline. In the future, we plan to extend our study to incorporate real-time decoding via a brain-computer interface (BCI) that rewards detection of high MW. As discussed above, and based on the demonstrated ability of BCI subjects to learn to volitionally modulate their brain rhythmic activity via operant conditioning [28], [36], we expect increasing classification performance as subjects practice.

V. Conclusion

The focus of this work was on studying plausible neural correlates of MW modulated by visual delay in an experimental setting where 9 users performed a pick-and-place task with the dVRK. Visual feedback was delivered either in real-time (no delay), with a short delay (150 ms), or with a long delay (500 ms). EEG band limited power analysis in the various delay conditions revealed an increase in θ band in frontal and parieto-occipital areas. Moreover, we observed

a decreasing trend in α power over occipital regions for the delayed conditions. In addition, we showed that for some of the subjects the exposure to the synthetic delays could be classified solely based on EEG data, highlighting the richness of brain signals in exhibiting signatures of MW evoked by visual delay. This paper provides the desired bedrock for closing the loop of surgeon-centered surgical robotics, taking into account the neural markers of mental workload that can be incorporated in various levels of control.

REFERENCES

[1] S. F. Atashzar and R. V. Patel, "Teleoperation for minimally invasive robotics-assisted surgery," in *The Encyclopedia of MEDICAL ROBOTICS: Volume 1 Minimally Invasive Surgical Robotics*, pp. 341–372, World Scientific, 2019.

[2] C. Nguan, B. Miller, R. Patel, P. P. Luke, and C. M. Schlachta, "Preclinical remote telesurgery trial of a da Vinci telesurgery prototype," *The International Journal of Medical Robotics and Computer Assisted Surgery*, vol. 4, no. 4, pp. 304–309, 2008.

[3] P. Farajiparvar, H. Ying, and A. Pandya, "A brief survey of telerobotic time delay mitigation," *Frontiers in Robotics and AI*, p. 198, 2020.

[4] A. M. H. Maghazil, *The use of the da Vinci surgical robotic system for telesurgery and telementoring*. University of California, Davis, 2012.

[5] T. Haidegger, J. Sándor, and Z. Benyó, "Surgery in space: The future of robotic telesurgery," *Surgical Endoscopy*, vol. 25, no. 3, pp. 681–690, 2011.

[6] S. F. Atashzar, M. Naish, and R. V. Patel, "Active sensorimotor augmentation in robotics-assisted surgical systems," in *Mixed and Augmented Reality in Medicine*, pp. 61–81, 2018.

[7] J. Guo, C. Liu, and P. Poignet, "A scaled bilateral teleoperation system for robotic-assisted surgery with time delay," *Journal of Intelligent & Robotic Systems*, vol. 95, no. 1, pp. 165–192, 2019.

[8] R. D. Dias, M. C. Ngo-Howard, M. T. Boskovski, M. A. Zenati, and S. J. Yule, "Systematic review of measurement tools to assess surgeons' intraoperative cognitive workload," *Journal of British Surgery*, vol. 105, no. 5, pp. 491–501, 2018.

[9] M. I. Klein, C. H. Lio, R. Grant, C. M. Carswell, and S. Strup, "A mental workload study on the 2d and 3d viewing conditions of the da Vinci surgical robot," in *Human Factors and Ergonomics Society Annual Meeting*, vol. 53, pp. 1186–1190, 2009.

[10] M. I. Klein, J. S. Warm, M. A. Riley, G. Matthews, C. Doarn, J. F. Donovan, and K. Gaitonde, "Mental workload and stress perceived by novice operators in the laparoscopic and robotic minimally invasive surgical interfaces," *Journal of Endourology*, vol. 26, no. 8, pp. 1089–1094, 2012.

[11] J. Weber, K. Catchpole, A. J. Becker, B. Schlenker, and M. Weigl, "Effects of flow disruptions on mental workload and surgical performance in robotic-assisted surgery," *World Journal of Surgery*, vol. 42, no. 11, pp. 3599–3607, 2018.

[12] C. Wu, J. Cha, J. Sulek, T. Zhou, C. P. Sundaram, J. Wachs, and D. Yu, "Eye-tracking metrics predict perceived workload in robotic surgical skills training," *Human Factors*, vol. 62, no. 8, pp. 1365–1386, 2020.

[13] T. Kim, P. Zimmerman, M. Wade, and C. Weiss, "The effect of delayed visual feedback on telerobotic surgery," *Surgical Endoscopy and Other Interventional Techniques*, vol. 19, no. 5, pp. 683–686, 2005.

[14] M. J. Lum, J. Rosen, T. S. Lendvay, M. N. Sinanan, and B. Hannaford, "Effect of time delay on telesurgical performance," in *IEEE Int Conf Robotics and Automation*, pp. 4246–4252, IEEE, 2009.

[15] M. Anvari, T. Broderick, H. Stein, T. Chapman, M. Ghodoussi, D. W. Birch, C. Mckinley, P. Trudeau, S. Dutta, and C. H. Goldsmith, "The impact of latency on surgical precision and task completion during robotic-assisted remote telepresence surgery," *Computer Aided Surgery*, vol. 10, no. 2, pp. 93–99, 2005.

[16] R. D. Madder, S. VanOosterhout, A. Mulder, J. Bush, S. Martin, A. J. Rash, J. M. Tan, J. L. Parker, A. Kalafut, Y. Li, *et al.*, "Network latency and long-distance robotic telestenting: Exploring the potential impact of network delays on telestenting performance," *Catheterization and Cardiovascular Interventions*, vol. 95, no. 5, pp. 914–919, 2020.

[17] G. Gonzalez, M. Agarwal, M. V. Balakuntala, M. M. Rahman, U. Kaur, R. M. Voyles, V. Aggarwal, Y. Xue, and J. Wachs, "Deserts: Delay-tolerant semi-autonomous robot teleoperation for surgery," in *IEEE Int Conf Robotics and Automation*, pp. 12693–12700, 2021.

[18] T. Zhou, J. S. Cha, G. Gonzalez, J. P. Wachs, C. P. Sundaram, and D. Yu, "Multimodal physiological signals for workload prediction in robot-assisted surgery," *ACM Transactions on Human-Robot Interaction*, vol. 9, no. 2, pp. 1–26, 2020.

[19] K. A. Guru, S. B. Shafiei, A. Khan, A. A. Hussein, M. Sharif, and E. T. Esfahani, "Understanding cognitive performance during robot-assisted surgery," *Urology*, vol. 86, no. 4, pp. 751–757, 2015.

[20] K. A. Guru, E. T. Esfahani, S. J. Raza, R. Bhat, K. Wang, Y. Hammond, G. Wilding, J. O. Peabody, and A. J. Chowriappa, "Cognitive skills assessment during robot-assisted surgery: Separating the wheat from the chaff," *BJU International*, vol. 115, no. 1, pp. 166–174, 2015.

[21] P. Kazanzidesf, Z. Chen, A. Deguet, G. S. Fischer, R. H. Taylor, and S. P. Dimaio, "An open-source research kit for the da Vinci® Surgical System," in *IEEE Int Conf Robotics and Automation*, pp. 6434–6439, 2014.

[22] M. Hwang, D. Seita, B. Thananjeyan, J. Ichnowski, S. Paradis, D. Fer, T. Low, and K. Goldberg, "Applying depth-sensing to automated surgical manipulation with a da Vinci Robot," in *2020 Int Symp Medical Robotics*, pp. 22–29, 2020.

[23] A. Delorme and S. Makeig, "EEGLAB: An open source toolbox for analysis of single-trial EEG dynamics including independent component analysis," *Journal of Neuroscience Methods*, vol. 134, no. 1, pp. 9–21, 2004.

[24] A. Barachant, S. Bonnet, M. Congedo, and C. Jutten, "Riemannian geometry applied to BCI classification," in *LVA-ICA*, 2010.

[25] F. Yger, M. Berar, and F. Lotte, "Riemannian approaches in brain-computer interfaces: A review," *IEEE Transactions on Neural Systems and Rehabilitation Engineering*, vol. 25, no. 10, pp. 1753–1762, 2017.

[26] S. Kumar, F. Yger, and F. Lotte, "Towards adaptive classification using riemannian geometry approaches in brain-computer interfaces," in *7th Int Winter Conf Brain-Computer Interface*, pp. 1–6, 2019.

[27] C. Jeunet, S. Debener, F. Lotte, J. Mattout, R. Scherer, and C. Zich, "Mind the traps! design guidelines for rigorous bci experiments," in *Brain–Computer Interfaces Handbook*, pp. 613–634, CRC Press, 2018.

[28] S. Perdikis, L. Tonin, S. Saeedi, C. Schneider, and J. d. R. Millán, "The Cybathlon BCI race: Successful longitudinal mutual learning with two tetraplegic users," *PLoS Biology*, vol. 16, no. 5, p. e2003787, 2018.

[29] K. Katahira, Y. Yamazaki, C. Yamaoka, H. Ozaki, S. Nakagawa, and N. Nagata, "EEG correlates of the flow state: A combination of increased frontal theta and moderate frontocentral alpha rhythm in the mental arithmetic task," *Frontiers in Psychology*, vol. 9, p. 300, 2018.

[30] R. Fernandez Rojas, E. Debie, J. Fidock, M. Barlow, K. Kasmarik, S. Anavatti, M. Garratt, and H. Abbass, "Electroencephalographic workload indicators during teleoperation of an unmanned aerial vehicle shepherding a swarm of unmanned ground vehicles in contested environments," *Frontiers in Neuroscience*, p. 40, 2020.

[31] M. Z. Zakrzewska and A. Brzezicka, "Working memory capacity as a moderator of load-related frontal midline theta variability in Sternberg task," *Frontiers in Human Neuroscience*, vol. 8, p. 399, 2014.

[32] W. van Winsun, J. Sergeant, and R. Geuze, "The functional significance of event-related desynchronization of alpha rhythm in attentional and activating tasks," *Electroencephalography and Clinical Neurophysiology*, vol. 58, no. 6, pp. 519–524, 1984.

[33] G. Pfurtscheller, C. Neuper, and W. Mohl, "Event-related desynchronization (ERD) during visual processing," *International Journal of Psychophysiology*, vol. 16, no. 2-3, pp. 147–153, 1994.

[34] R. Chavarriaga, A. Sobolewski, and J. d. R. Millán, "Errare machinale est: The use of error-related potentials in brain-machine interfaces," *Frontiers in Neuroscience*, p. 208, 2014.

[35] E. Formaggio, S. F. Storti, I. Boscolo Galazzo, M. Gandolfi, C. Geroin, N. Smania, L. Spezia, A. Waldner, A. Fiaschi, and P. Manganotti, "Modulation of event-related desynchronization in robot-assisted hand performance: Brain oscillatory changes in active, passive and imagined movements," *Journal of Neuroengineering and Rehabilitation*, vol. 10, no. 1, pp. 1–10, 2013.

[36] S. Perdikis and J. d. R. Millán, "Brain-machine interfaces: A tale of two learners," *IEEE Systems, Man, and Cybernetics Magazine*, vol. 6, no. 3, pp. 12–19, 2020.